On the Effect of Porous Layers on Melting Heat Transfer in an Enclosure

E. A. Ellinger* and C. Beckermann
Department of Mechanical Engineering, The University of Iowa, Iowa City, Iowa

■An experimental study is reported of melting of a pure substance in a vertical rectangular enclosure that is partially occupied by horizontal or vertical layers of a relatively high thermal conductivity porous medium. To enhance heat transfer, the porous layers are located in regions where the melting rates for a pure substance are the lowest. *n*-Octadecane is used as the phase-change material, and the porous matrix is composed of glass or aluminum beads of various diameters. Natural convection in the liquid and conduction in the solid are present. The temperature distributions in both the fluid and porous regions are measured using thermocouple rakes, and solid-liquid interface positions and shapes are recorded by tracing the interface at specified time intervals. It is found that the differences in the thermophysical properties between the porous layer and the pure fluid layer cause strong variations in heat transfer, melt convection, and the movement and shape of the solid-liquid interface. Although a porous layer may cause a faster movement of the solid-liquid interface, the melting and heat transfer rates are reduced compared to the case without a porous layer. This is attributed to the effects of the low porosity and permeability of the porous media tested, which are not offset by the high thermal conductivity of the media. Considerable care must be exercised in trying to enhance melting heat transfer using high thermal conductivity porous media.

Keywords: *melting, porous media, thermal energy storage, natural convection*

INTRODUCTION

Latent heat thermal energy storage devices have attracted considerable interest because of their large potential for energy savings and their ability to provide or absorb thermal energy at an essentially constant temperature. Because most phase-change materials used in such thermal energy storage devices have a relatively low thermal conductivity, means of enhancing the heat transfer between the solid-liquid interface and some heat exchanger surface have been investigated [1]. For both industrial [2] and space power [3, 4] applications, it has been proposed that the heat transfer rate be increased by embedding a high thermal conductivity porous medium into the phase-change material. The effects of a porous medium on the heat transfer and phase-change rates have not been investigated in detail. The presence of the porous medium can considerably reduce the thermal energy storage capacity of a canister of a given volume. Also, although a high thermal conductivity porous medium can be expected to enhance the heat transfer by conduction and cause a faster solid-liquid interface motion, it will also impede the fluid flow in the melt region, thereby reducing the heat transfer by natural convection inside a thermal energy storage canister. In this study, it is proposed to fill only part of the canister with the porous medium in order to counteract the reductions in the storage capacity and the natural convection heat transfer due to the porous medium.

The present study considers melting of a pure substance inside a vertical rectangular enclosure partially occupied by horizontal or vertical layers of various saturated porous media (see Fig. 1). Porous media of relatively low porosity (beads, $\epsilon = 0.38$) are considered in order to emphasize the effects of reduced storage capacity. By choosing special porous layer configurations and relatively high thermal conductivity porous materials, it is hoped to enhance the heat transfer, particularly in those regions of a canister where the melting rates are the lowest (ie, in the lower half of the enclosure during convection-dominated melting and far away from the heated wall). From a more fundamental point of view, it is of interest to investigate the effect of the abrupt transition in the thermophysical properties across the pure substance-porous medium interface on the solid-liquid interface shape and motion. In addition to enhanced thermal energy storage systems, other applications may include casting of composite materials by melt infiltration of a fiber perform and thawing and freezing of soil in the presence of a body of water.

Although no studies of solid-liquid phase change of adjacent layers of a pure substance and a porous medium have been reported in the literature, work in several areas bears direct relevance to the case considered in this paper. Solid-liquid phase change of pure substances has been exten-

* Research assistant; presently employed by Caterpillar, Inc., Peoria, Illinois.

Address correspondence to Professor C. Beckermann, Department of Mechanical Engineering, The University of Iowa, Iowa City, IA 52242.

Experimental Thermal and Fluid Science 1991; 4:619-629

0894-1777/91/$3.50

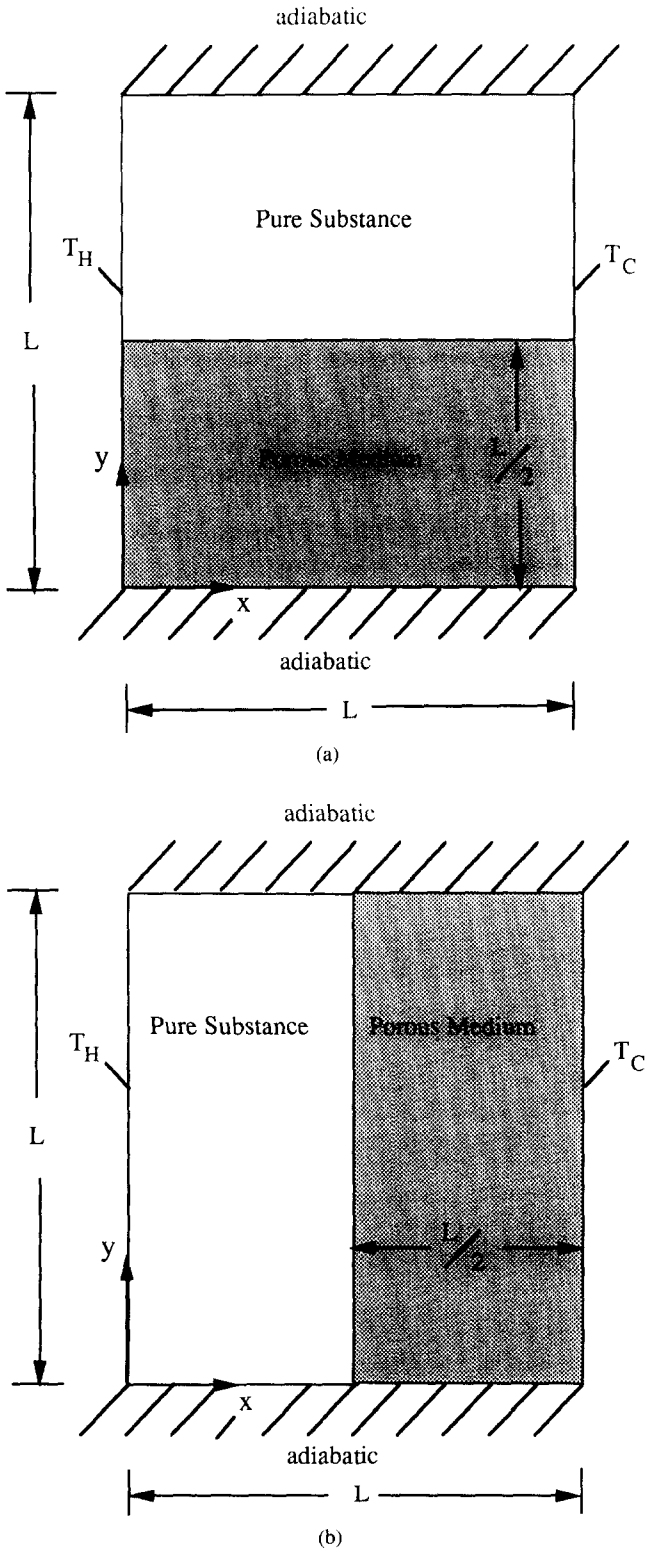

Figure 1. Configurations considered in the present study. (a) Horizontal porous layer; (b) vertical porous layer.

sively studied, and several comprehensive reviews are available [5–7]. The influence of thermally induced natural convection on the solid–liquid interface shape and motion inside a vertical rectangular cavity has been well documented [8–10]. On the other hand, relatively little work has been reported on solid–liquid phase change in porous media. Numerical analyses and experiments have been performed of freezing and thawing around vertical freeze pipes [11, 12] and of melting and solidification of liquid-saturated porous media in rectangular cavities (see, for example, Refs. 13 and 14). Studies of natural convection in adjacent layers of a pure fluid and a porous medium lend insight into the influence of the abrupt change of thermophysical properties between pure and porous layers on natural convection flow and heat transfer. It has been established that a high thermal conductivity and/or low permeability porous layer will suppress fluid flow in the porous layer and result in strong cusps in the streamline and isotherm patterns at the porous–fluid layer interface [15, 16]. Beckermann et al [17] conducted a numerical and experimental study of natural convection in adjacent horizontal and vertical pure and porous layers consisting of glass and aluminum beads. They found that there was relatively little fluid flow in the porous layers for the porous media that were studied.

In the present study, melting experiments are performed in a rectangular test cell. These experiments are listed in Table 1. *n*-Octadecane is used as the phase-change material, and half of the test cell is occupied by either a vertical or a horizontal layer of a porous medium consisting of glass or aluminum beads saturated with *n*-octadecane. These porous media have an effective thermal conductivity that is between 4 and 40 times as high as the thermal conductivity of *n*-octadecane (see Table 1). A reference experiment without a porous layer is also conducted. The two vertical side walls of the test cell are held at temperatures above and below the melting temperature. This causes natural convection in the melt region as well as heat conduction in the solid phase-change material. The top, bottom, front, and back walls are well insulated. Figure 1 illustrates the physical configuration considered.

EXPERIMENTS

Test Cell

The rectangular test cell had inner dimensions of 20.32 cm (height) × 20.32 cm (width) × 15.24 cm (depth). A detailed description of the test cell appears elsewhere [18]. Each side wall consisted of a multipass heat exchanger machined from a copper plate. An alcohol–water mixture was circulated through the heat exchangers from two constant-temperature baths in order to maintain isothermal boundary conditions on the side walls. Each heat exchanger had three sections through which the flow rate could be controlled independently. Eight thermocouples were soldered very near the surface of each heat exchanger to monitor the temperatures of the vertical side walls. In all experiments, the temperatures of the heat exchangers were uniform to within $\pm 0.1^\circ C$. The bottom plate was milled from phenolic sheet, and the front, back, and top walls were made of Lexan plates to allow for visual observation. Holes were drilled near the edges of the top plate to allow excess fluid to drain from the test cell in response to density differences between the liquid and solid phases. The entire test cell and flow control system was covered with 6 cm elastomer foam insulation.

Nine thermocouple rakes, used to measure the temperature distribution within the test cavity, were hung from an aluminum frame surrounding the test cell. Each rake was made from a 0.21 cm stainless steel tube to which three perpendicu-

Table 1. List of Experimental Conditions (T_f = 28.0°C)

Expt.	T_H (°C)	T_C (°C)	T_i (°C)	*Config.*	d_b (mm)	*Bead*	ϵ	$Ra \times 10^{-9}$	*Pr*	*Ste*	$Da \times 10^7$
1	42.9	13.0	13.0	—	—	none	—	6.411	50.32	0.271	—
2	42.9	13.0	14.6	Horiz.	11.02	glass	0.42	6.415	50.32	0.271	22.720
3	42.9	13.0	13.1	Horiz.	5.98	glass	0.35	6.413	50.32	0.271	3.553
4	42.9	13.0	13.3	Horiz.	6.35	alum.	0.38	6.413	50.32	0.271	3.194
5	42.9	13.0	13.1	Vert.	5.98	glass	0.35	6.420	50.31	0.271	3.553
6	42.9	13.0	13.0	Vert.	6.35	alum.	0.38	6.415	50.32	0.271	3.194

Expt.	Ω (ϵ = 1, γ = 0)	Ω (ϵ, γ = 1)	Ω (ϵ, γ = 0)	Λ (ϵ = 1, γ = 0)	Λ (ϵ, γ = 1)	Λ (ϵ, γ = 0)
1	0.929	—	—	2.486	—	—
2	0.929	1.197	1.168	2.486	4.346	4.970
3	0.929	1.069	1.044	2.486	4.749	5.270
4	0.929	1.282	1.255	2.486	17.603	41.669
5	0.929	1.069	1.044	2.486	4.750	5.270
6	0.929	1.282	1.255	2.486	17.603	41.669

lar arms of 0.13 cm stainless steel tubing were epoxied. The thermocouple junctions were at the tip of each arm, and the thermocouple rakes were hung such that the arms were perpendicular to the main heat and fluid flow direction. The thermocouple junctions were placed along the vertical center plane of the test cell, resulting in three levels of nine thermocouple junctions at distances of 2.54, 10.16, and 17.78 cm from the floor of the test cell chamber. The error in the placement of the thermocouples was estimated to be less than ±1 mm in both the horizontal and vertical directions. By monitoring the temperature of a thermocouple as the solid-liquid interface passed it (the temperature at this point is known to be the fusion temperature, 28.0°C), the temperature readings were determined to be accurate to ±0.1°C. To examine the influence of the thermocouple rakes on the heat transfer and fluid flow, experiments were performed without the rakes, and the results were found to be very close to the ones with the rakes present [18].

Test Materials

The phase-change material (PCM) used in this study was research grade, 99% pure *n*-octadecane. Soda lime glass beads and aluminum beads were used to form the porous matrix. Thermophysical properties of the *n*-octadecane and the glass and aluminum beads are listed elsewhere [18]. Measured values of the average bead diameters and the porosity of the porous layers are provided in Table 1.

Experimental Procedures

To prepare the test cell for the melting experiments, the temperatures of the heat exchangers were lowered to approximately 0°C, and liquid *n*-octadecane was added in 1 cm layers. Each layer was allowed to freeze almost completely before the next layer was added. This process eliminated the complicated dendritic structures and large amount of entrapped air that characterize solidification of large amounts of *n*-octadecane. For the vertical porous layer experiments, a galvanized steel screen was inserted in the test cell to support the beads. Observations indicated that the screen had a negligible influence on the heat transfer and fluid flow processes.

When the entire test cell had been filled, the desired initial temperature, $T_i = T_C$, was established in the test cell by circulating fluid through both heat exchangers from one constant-temperature bath. Owing to small heat losses from the test cell, it was impossible to bring the material in the test cell to a uniform initial temperature. Thus, the temperature T_i listed in Table 1 represents the average initial temperature. The standard deviation from the initial temperature was about ±0.5°C, with a maximum deviation of 1.5°C. This results in an uncertainty of about 3% in the initial subcooling below the melting temperature. These nonuniformities are not expected to have a significant influence on the subsequent experiment because both the left and right walls were held at fixed temperatures. It was estimated that the heat losses from the test cell were only a few percent of the average heat transfer rates at the heat exchangers during the experiments [18]. The other constant-temperature bath was set to a few degrees above the desired hot-wall temperature to compensate for the very high heat flux at the hot wall at the beginning of the experiment. At time $t = 0$, the valves were switched and the fluids from the hot and cold constant-temperature baths were circulated through the hot and cold wall heat exchangers, respectively. Typically, it took 5 min for the hot wall to reach the desired temperature, T_H, for an experiment of approximately 40 h. Except for a few random fluctuations, the wall temperature stayed within ±0.2°C of the average values T_H and T_C listed in Table 1.

Temperatures measured by the 16 wall thermocouples and the 27 interior thermocouples were recorded by an HP 3852S data logger. Readings were taken every 15 s at the beginning of the experiment to adequately monitor initial transients. The scanning interval was gradually increased to 10 min.

In addition to the temperature data, solid-liquid interface positions were recorded by placing a square transparency on the back wall and tracing the interface at appropriate intervals. For this purpose, the insulation covering the back wall was temporarily removed. The tracings were estimated to be accurate to within ±1.5 mm in the horizontal and vertical directions. Better accuracy was not possible owing to the presence of the beads in the porous layer. In all experiments, the melt region had a very uniform thickness over the depth of the test cell (of the order of 1 mm), indicating that three-dimensional effects were not too important. The melt volume fraction, the amount of melted PCM divided by the

total volume of the cavity, was obtained by measuring the area under each solid-liquid interface tracing and dividing that area by the total cross-sectional area of the test cell. The area corresponding to the melted PCM inside the porous medium was first multiplied by the porosity of the porous medium listed in Table 1.

RESULTS AND DISCUSSION

As shown in Table 1, melting experiments were performed for the case of a pure fluid (Experiment 1), horizontal layers of large glass, small glass, and small aluminum beads (Experiments 2, 3, and 4, respectively), and vertical layers of small glass and small aluminum beads (Experiments 5 and 6, respectively).

Through a normalization of the governing conservation equations [14], it is found that the dimensionless parameters Ra, Pr, Ste, and Da and the property ratios Ω and Λ govern solid-liquid phase change of pure and porous media in cavities of square cross-section. These quantities are defined as follows:

$$Ra = \frac{g\beta(T_H - T_C)L^3}{\nu_l \alpha_l} \qquad Pr = \frac{\nu_l}{\alpha_l} \qquad Ste = \frac{c_l(T_H - T_C)}{\Delta h}$$

$$Da = K/L^2 \qquad \Omega = \overline{\rho c}/\rho_l c_l \qquad A = k_{\text{eff}}/k_l \qquad (1)$$

To obtain these quantities, the thermophysical properties were evaluated at the mean temperature of the relevant phase. The permeability was calculated utilizing the Kozeny-Carman equation [14]. The mean thermal capacitance is defined as

$$\overline{\rho c} = \epsilon\rho_{\text{pcm}}[\gamma c_l + (1 - \gamma)c_s] + (1 - \epsilon)\rho_p c_p \qquad (2)$$

where $\gamma = 1$ in the melt region and $\gamma = 0$ in the solid region. ϵ is the porosity of the porous medium and is equal to unity in the pure fluid layer. For simplicity, the solid and liquid densities are assumed to be equal and are denoted by ρ_{pcm}. In the following, k_{pcm} denotes the thermal conductivity of either the liquid or the solid *n*-octadecane and is calculated from

$$k_{\text{pcm}} = \gamma k_l + (1 - \gamma)k_s \qquad (3)$$

In the literature, several models for calculating the effective thermal conductivity of a saturated porous medium have been reported. In the experiments with the soda lime glass beads, the difference in thermal conductivity between the porous matrix and the PCM is not too great, and the series model was used, that is,

$$k_{\text{eff}} = \epsilon k_{\text{pcm}} + (1 - \epsilon)k_p \qquad (4)$$

However, in the case of *n*-octadecane and aluminum beads, the Veinberg model [19], which is valid for a medium with randomly distributed spherical inclusions, was found to be more appropriate [17]; that is,

$$k_{\text{eff}} + \epsilon\left[\frac{k_p - k_{\text{pcm}}}{k_{\text{pcm}}^{1/3}}\right]k_{\text{eff}}^{1/3} - k_p = 0 \qquad (5)$$

Since the liquid fraction γ and hence the property ratios are a function of time, the values for Ω and Λ listed in Table 1 are those for the limiting cases: a pure solid ($\epsilon = 1$, $\gamma = 0$), a porous medium with the PCM completely liquid (ϵ, $\gamma = 1$), and a porous medium with the PCM completely solid (ϵ, $\gamma = 0$).

For each of the experiments listed in Table 1, tracings of the solid-liquid interfaces (Fig. 2), a steady-state temperature profile (Fig. 3), and a graph of melt volume fraction versus time (Fig. 4) are presented. Note that all the experiments were conducted with a temperature of 42.9°C at the hot wall and 13.0°C at the cold wall and therefore have the same Rayleigh, Prandtl, and Stefan numbers. In addition, the relationship between the dimensional time t and nondimensional time Fo Ste is $t = (1.732 \times 10^6 \text{ s})$ (Fo Ste) for all experiments. The nondimensional fusion temperature (or subcooling number [7]) for all experiments is approximately equal to 0.5; that is, the fusion temperature was midway between the hot and cold-wall temperatures. Although the pure liquid and solid properties k, ρ, and c are approximately the same for all experiments, the effective property ratios Ω and Λ are different owing to the presence of different types of porous media. The differences in the results between the experiments for each configuration are therefore due to porosity, permeability, and effective thermal conductivity variations.

Interface Tracings

Experiment 1 consisted of melting pure *n*-octadecane. The progression of the interface with time for this experiment is presented in Fig. 2*a*. The interface shapes are reminiscent of those observed by Bénard et al [10], who conducted a similar experiment. The vertical shape of the interface at Fo Ste = 1.34×10^{-3} indicates that in the early stages of the experiment, heat transfer across the small melt layer is primarily by conduction. The curvature at the top of this interface indicates the onset of natural convection in this region.

In the following stages of the experiment, the solid-liquid interface moves faster at the top of the cavity than at the bottom, indicating the presence of natural convection in the upper portion of the melt region. Fluid is heated as it rises along the hot wall, then impinges on the top plate, and cools as it descends along the interface. In this way, heat is transferred from the hot wall to the interface. Boundary layers develop along the hot wall and the solid-liquid interface, and the stagnant center core of the melt region becomes thermally stratified. The fluid is hottest at the top of the cavity, and thus the *n*-octadecane melts fastest in this region.

As the melt region thickens and the solid region narrows, the thermal resistance of the solid region decreases, so the heat transfer rate across the solid region increases. On the other hand, the natural convection heat transfer rate across the melt region is quasi-steady [10, 20]. As the heat fluxes on the liquid and solid sides of the solid-liquid interface approach each other, the movement of the interface slows down and eventually ceases. The heat fluxes through the solid and liquid first become equal near the top of the cavity where the thickness of the melt region is the greatest. Therefore, the upper portion of the solid-liquid interface reaches its steady-state position before the lower portion does.

At the bottom of the test cell, the solid-liquid interface tracings curve slightly before they intersect the bottom wall. This may be the result of a small heat gain because of x-direction conduction in the bottom plate. In all experiments, however, the volume melted due to this slight curvature is no greater than about 2% of the total melted volume at a given time.

A time history of the solid–liquid interface positions of the experiment involving the horizontal layer of large glass beads, Experiment 2, is presented in Fig. 2*b*. It can be seen that the interface movement in the porous layer is faster than in the pure fluid layer only in the conduction-dominated period at the beginning of the experiment (see the interfaces at Fo Ste = 0.91×10^{-3} and 2.10×10^{-3}). But, by the time Fo Ste = 5.09×10^{-3}, the solid–liquid interface has progressed much further in the upper half of the cavity than in the lower half of the cavity, owing to natural convection.

Comparing Experiment 1 (melting of pure *n*-octadecane) and 2, the influence of the porous layer in Experiment 2 manifests itself mainly through a different interface shape and movement in the porous region. The residual solid in Experiment 2 eventually takes on a triangular shape and is much larger in volume than the residual solid in Experiment 1. This is due to weaker natural convection in the porous medium as a result of (1) the somewhat higher effective thermal conductivity of the porous layer compared to the pure layer and (2) the lower permeability of the porous medium compared to the pure liquid case (with an infinitely large permeability). Beckermann et al [17] found that natural convection is relatively weak within a horizontal porous layer of glass beads superposed by a fluid layer for a cavity heated or cooled from the sides. This is also further supported through the temperature profiles presented in the next section.

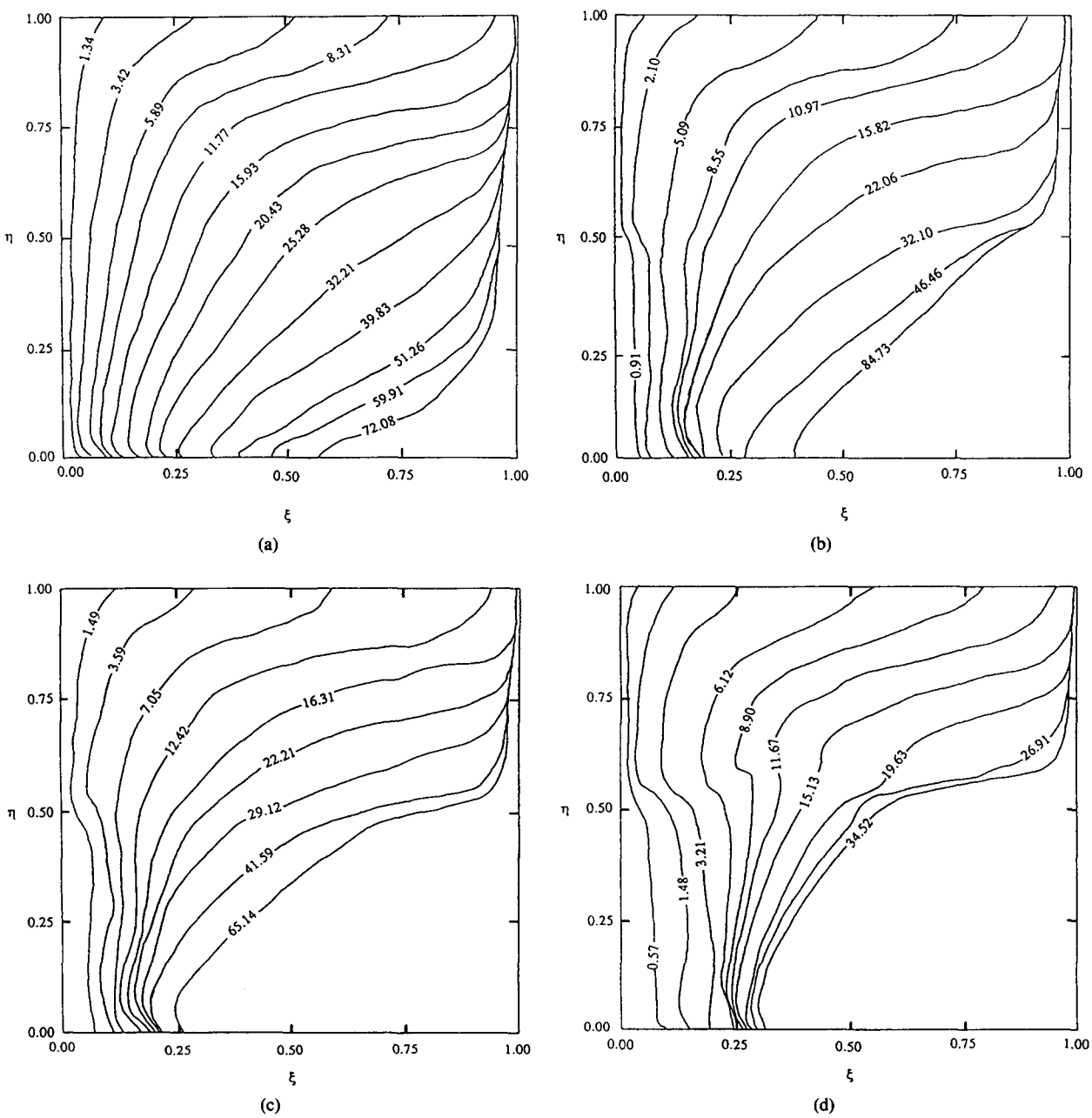

Figure 2. Solid–liquid interface tracings at specified Fo Ste $\times 10^3$. (a) Experiment 1; (b) Experiment 2; (c) Experiment 3; (d) Experiment 4; (e) Experiment 5; (f) Experiment 6.

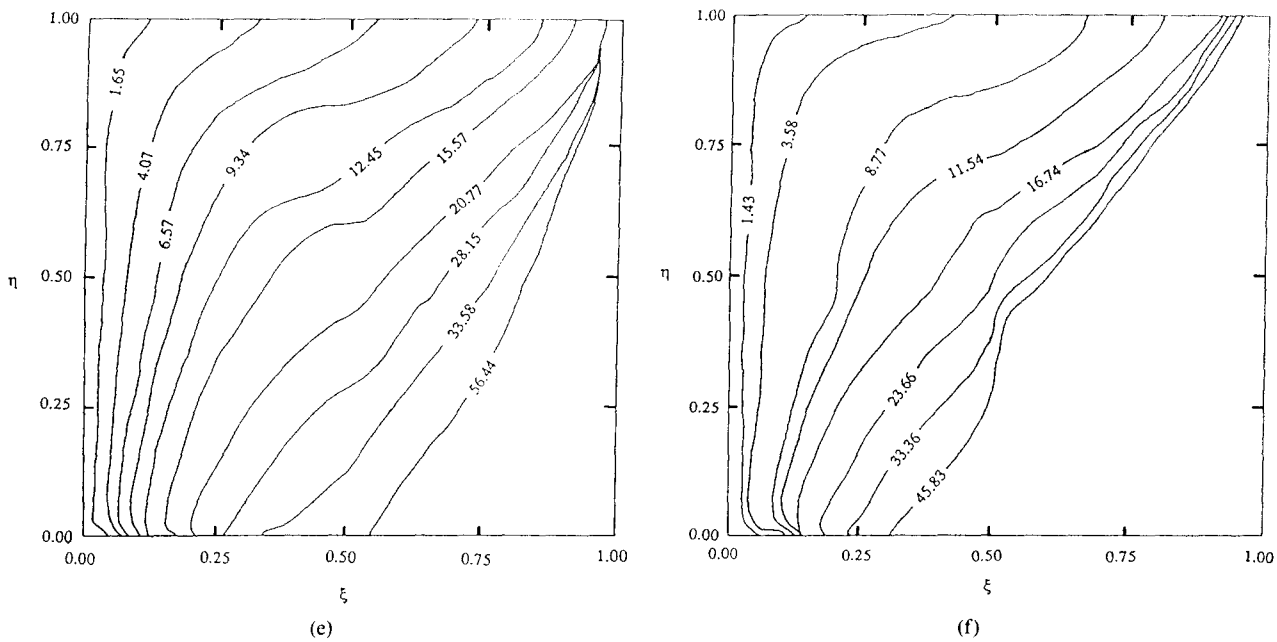

Figure 2. (*Continued*)

In Experiment 3, the lower half of the test cell is filled with a horizontal layer of small glass beads. Although the bead properties ρ, c, and k are the same as those of the large glass beads used in Experiment 2, the layer of small glass beads has a much lower permeability (see Table 1). Figure 2*c* illustrates that initially in Experiment 3, the interface moves faster in the porous layer than in the pure layer. At later times, the heat transfer is characterized by strong convective flow in the fluid layer, which causes faster melting at the top of the test cell than at the bottom. These features are identical to the case of melting of a horizontal layer of large glass beads. However, it is evident from Figs. 2*b* and 2*c* that there are differences between Experiments 2 and 3. In the case of the small glass beads, there is a larger region of unmelted solid at all times in the porous layer than in the case of the large glass beads. This is the result of weaker natural convection in the porous region of Experiment 3 than in Experiment 2 because of the lower permeability, which impedes convective flow.

In Experiment 4, the lower half of the test cell was filled with a horizontal layer of aluminum beads. It was expected that the high thermal conductivity of the aluminum would play an important role in Experiment 4. The porosity and permeability of the aluminum beads are approximately the same as those of the small glass beads. Hence, the major difference between the porous layers used in Experiments 3 and 4 is their effective thermal conductivities. The interface tracings for Experiment 4, shown in Fig. 2*d*, show the strong influence of the high thermal conductivity porous medium during the conduction-dominated region at the beginning of the experiment. The rapid initial movement of the solid-liquid interface through the small aluminum bead porous layer, as compared to the solid-liquid interface movement in the pure layer, continues for a greater portion of the experiment than in the case of the horizontal layer of small glass beads (Experiment 3). Even when convection begins to dominate the heat transfer in the fluid layer, the interface in the porous layer is still vertical, and a point of inflection in the solid-liquid interface is present at the interface between the pure fluid and porous medium layers. Owing to the convection in the fluid layer, the interface movement at later times, however, is much faster in the upper portion of the cavity than in the porous layer, despite the high effective thermal conductivity of the porous layer. Therefore, filling of the entire test cell with aluminum beads would result in a lower overall melting rate. The more vertical solid-liquid interface shape in the small aluminum bead porous medium and the larger size of the remaining solid at steady state, compared to the case of the small glass beads (Experiment 3), are both due to the higher effective thermal conductivity, which weakens the convective flow in the melt portion and decreases the thermal resistance across the solid portion of the porous layer.

In Experiments 5 and 6, the right half of the test cavity is filled with layers of small glass and aluminum beads, respectively. Representative interface tracings for Experiment 5 are shown in Fig. 2*e*. As expected, the interface shapes look similar to those in the case of melting of the pure *n*-octadecane (Fig. 2*a*) at early times in the experiment. The interface shapes and melting rates are not completely identical in Experiments 1 and 5 at early times, because the solid region in Experiment 5 has a somewhat lower thermal resistance due to the presence of the porous layer. When the solid-liquid interface crosses the pure fluid-porous medium interface at $\xi = 0.5$, a point of inflection appears in the interface shape, as can be seen near the top of the interface at Fo Ste $= 9.34 \times 10^{-3}$ in Fig. 2*e*. This is mainly because of the abrupt change in permeability at the pure fluid-porous medium interface. As the solid-liquid interface moves further into the porous medium, it assumes a more linear shape due to the weaker convective flow in the porous layer compared to the pure fluid layer. The weak natural convection in the porous layer causes the thickness of the remaining solid adjacent to the cold wall near the top of the test cell to be greater than in

the previous experiments when this region was composed of pure fluid. At steady state the solid-liquid interface is completely within the porous layer and has assumed a very linear shape as a result of the weak natural convection in this region.

Experiment 6 differs from Experiment 5 in that the vertical porous layer consists of aluminum beads and therefore has a much higher effective thermal conductivity (see Table 1). Solid-liquid interface tracings for Experiment 6 are displayed in Fig. 2*f*. Initially, the solid-liquid interface shapes are quite similar to those for a vertical layer of small glass beads. As in Experiment 5, a point of inflection appears in the solid-liquid interface shape at the pure fluid-porous medium interface owing to abrupt property changes. The principal difference in the history of the solid-liquid interface shapes shown in Fig. 2*e* (Experiment 5) and Fig. 2*f* (Experiment 6) is that in the case of the vertical layer of aluminum beads the solid-liquid interface movement ceases sooner than in the case of the vertical layer of glass beads. The resulting large mass of residual solid left in the test cell is due to the high effective thermal conductivity of the aluminum bead layer, which weakens natural convection in the porous layer and reduces the thermal resistance across the solid region. At steady state, the solid-liquid interface is partly in the pure

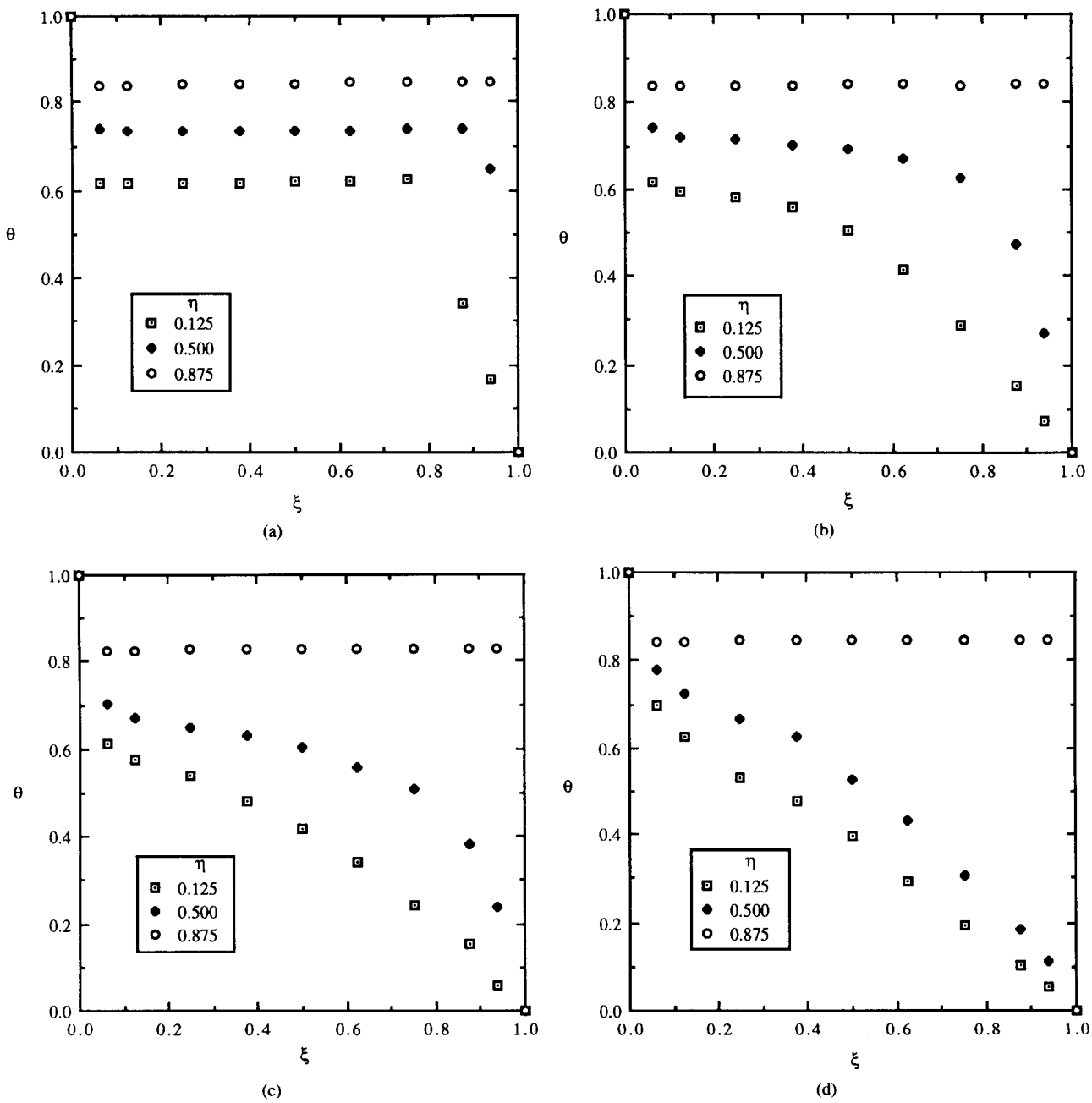

Figure 3. Steady-state temperature profiles. (a) Experiment 1; (b) Experiment 2; (c) Experiment 3; (d) Experiment 4; (e) Experiment 5; (f) Experiment 6.

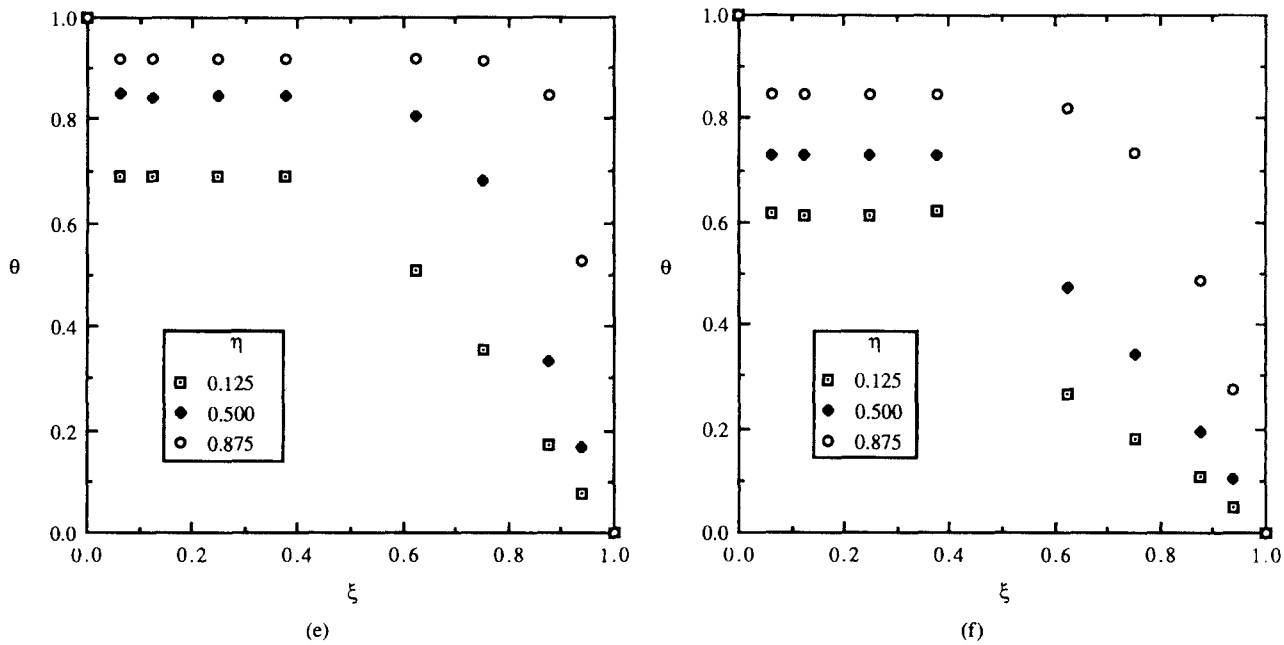

Figure 3. (*Continued*)

layer and partly in the porous layer. In the porous layer its shape is linear, whereas in the pure layer its curved shape is similar to that found in Experiment 1.

Steady-State Temperature Profiles

The steady-state temperature profiles for the case of melting of pure *n*-octadecane, shown in Fig. 3*a* (t = 4121 min), reveal evidence of strong natural convection in the melt region. The core of the melt region is thermally stratified, and thin thermal boundary layers are present along the hot wall and the solid-liquid interface. Only the two far right thermocouples at the η = 0.125 level are embedded in solid (ie, $\theta < 0.5$), which is in agreement with the interface tracing of Fig. 2*a*.

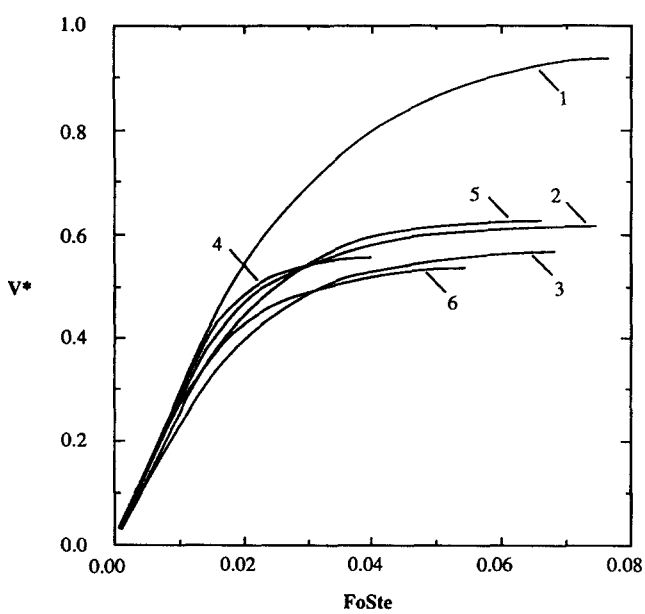

Figure 4. Melt volume fraction variations with time for Experiments 1-6.

The steady-state temperature distribution for Experiment 2 is presented in Fig. 3*b*. The profile in the melted portion of the porous layer at the η = 0.125 level shows a more linear variation between the hot wall and the interface, indicating that the convective flow in the porous layer is relatively weak. The temperature profile at the η = 0.500 level is more horizontal than at the 0.125 level, because it lies on the interface of the pure fluid and porous regions and is influenced by the convective flow in the upper region. The temperature profile in the pure fluid region (η = 0.875) in Fig. 3*b* (Experiment 2) shows approximately the same temperatures as the temperature profile at the same level in Fig. 3*a* (Experiment 1), implying that the convective flow in the upper region is not strongly influenced by the presence of the porous medium in the lower region. Again, the interface position that can be inferred from the temperature profiles coincides well with the one shown in Fig. 2*b*.

The steady-state temperature profile for Experiment 3, presented in Fig. 3*c*, shows that the lower permeability of the small glass heads impedes the convective flow even more and produces more linear temperature profiles in the melt portion of the porous layer (η = 0.125 and 0.500) than in the case of the large glass beads (Fig. 3*b*). The horizontal temperature profile at the η = 0.875 level, however, is identical in Figs. 3*b* and 3*c*, indicating that the heat transfer in the pure layer is not strongly affected by the difference in permeability between the layers of large and small glass beads.

The domination of conduction in the aluminum bead porous layer is further corroborated by the steady-state temperature profiles for Experiment 4, shown in Fig. 3*d*. The temperature profiles at both the η = 0.125 and 0.500 levels are

almost linear throughout the melt and solid regions except very close to the hot wall, where there is a thermal boundary layer due to weak convective flow. The temperatures at the $\eta = 0.875$ level are only slightly lower than in Experiment 3, indicating that the porous layer effective thermal conductivity has only a slight influence on the convection in the fluid layer.

The steady-state temperature profile for Experiment 5 is depicted in Fig. 3*e*. Note that in Experiment 5 and 6 involving a vertical porous layer, the presence of the screen at the $\xi = 0.5$ position prevented the center thermocouple from being installed. It can be seen that the natural convection in the porous layer is weaker than in the pure layer; the temperature profile at the $\eta = 0.875$ level in this region is no longer horizontal, and the temperature profile at $\eta = 0.125$ is very linear. The temperature field is fully stratified in the left half of the cavity with the core pushed toward the top of the cavity, compared to the steady-state temperature profile in the melt region for the case of melting of pure *n*-octadecane, as shown in Fig. 3*a*.

An examination of the steady-state temperature profile for the case of a vertical layer of small aluminum beads (Experiment 6), shown in Fig. 3*f*, reveals that a greater part of the temperature drop across the test cavity occurs in the pure fluid, because of the high effective thermal conductivity of the aluminum bead layer. Therefore, the temperatures in the core of the pure fluid region are shifted downward from the values for the case of the glass bead layer (Experiment 5).

Melt Volume Fraction

A history of the melt volume fraction variation for each experiment is presented in Fig. 4. The melting rate (ie, the slopes of the curves in Fig. 4) is a direct indication of the heat transfer rates at the hot and cold heat exchangers, because the Stefan numbers for the present experiments (see Table 1) are small enough that the thermal inertia of the liquid and solid can be neglected [**20**]. For small Stefan numbers, an energy balance on the enclosure shows that the difference between the heat transfer rates at the hot and cold walls is directly proportional to the melting rate.

It can be seen that the growth of the melt region for Experiment 1 proceeds through a short initial nonlinear period and becomes linear until about Fo Ste = 0.02. During the initial conduction regime, the melt volume is expected to increase with the square root of time, which is consistent with the fact that the linear portion of the curve does not extend through the origin of Fig. 4. The conduction-dominated regime is very short because of the relatively high value of the Rayleigh number. The following linear melt volume fraction variation is typical of the convection-dominated melting regime [**10**, **20**]. It should be noted that during the conduction- and convection-dominated melting regimes, heat conduction through the solid region has a negligible influence on the melting rates. After Fo Ste = 0.02, the slopes of the curve starts to decrease as the movement of the solid-liquid interface slows down, which is due to the decreasing thermal resistance of the solid region and therefore increasing heat transfer through the solid away from the solid-liquid interface. Eventually the curve becomes horizontal as the heat transfer rates through the solid and liquid are balanced and steady state is approached. Note that V^* never reaches unity because the cold (right) wall is held below the fusion temperature. Similar observations have been made by Beckermann and Viskanta [**20**] for melting of gallium.

From a comparison of Experiments 1 and 2, it can be seen that the presence of the horizontal layer of large glass beads results in a slightly lower melting rate during the convection-dominated regime. In other words, the heat transfer at the hot wall is somewhat reduced, although the effective thermal conductivity of the porous layer is more than four times as high as the thermal conductivity of the pure PCM (see Table 1). This can be attributed to the reduction in the natural convection intensity in the lower half of the test cell due to the porous medium. In addition, the presence of the porous medium increases the distance between the hot wall and the solid-liquid interface for a given volume of PCM melted. The resulting increase in the thermal resistance of the melt region counteracts the decrease due to the higher thermal conductivity. The porous layer also inhibits melting at later times, and Experiment 2 approaches steady state more quickly than Experiment 1. The large difference in the final melt volume fractions between Experiments 1 and 2 is a clear indication of both the reduced heat transfer across the melt region and, particularly, the lower thermal energy storage capacity in Experiment 2.

Since the permeability of the porous layer in Experiment 3 is much lower than in Experiment 2, the effects of the natural convection heat transfer reduction are even more pronounced. The melting rate in Experiment 3 is lower than in Experiment 2, whereas the residual volume of solid in the test cell is larger.

Although convective flow is virtually nonexistent in the porous layer of Experiment 4, the high effective thermal conductivity of the aluminum bead layer results in the same melting rate as in Experiment 1 until about Fo Ste = 0.015. At that point, conduction through the solid reduces the melting rate, and Experiment 4 reaches steady state at about Fo Ste = 0.03. It is important to note that until Fo Ste = 0.015 the solid-liquid interface in Experiment 4 moves at a faster rate than in Experiment 1. However, the presence of the porous medium in Experiment 4 results in approximately the same volume of PCM melted in Experiments 1 and 4 at Fo Ste = 0.015, indicating that the total heat transfer rates at the hot wall are the same until that time.

Experiments 5 and 6 show, as expected, an almost identical melt volume fraction variation as Experiment 1 until about Fo Ste = 0.01. At Fo Ste = 0.01, part of the solid-liquid interface enters the vertical porous layers in these experiments, causing a marked decrease in the melting rate relative to Experiment 1, which can be attributed to the low natural convection intensity in the porous layers. Experiment 6 has a significantly lower final melt volume fraction than Experiment 5 owing to increased heat conduction in the solid region of the aluminum bead layer.

PRACTICAL SIGNIFICANCE

The present study clearly shows that considerable care must be exercised in trying to enhance heat transfer in thermal energy storage systems by using high thermal conductivity porous media. The porous medium not only reduces the storage capacity of a given canister but also decreases the heat transfer by natural convection. For the horizontal layers, only the experiment with the aluminum beads resulted in melting rates comparable to those attained without a porous

medium. Although such a porous layer causes the solid-liquid interface to move faster, the volume of PCM melted and thus the heat transfer rate at the heated wall are not enhanced by the presence of the porous medium. Furthermore, filling the entire test cell with aluminum beads would result in a lower melting rate, because the convection in the upper portion of the cavity would be suppressed. In practice, a porous medium with a higher porosity and permeability, such as an aluminum foam, should be used. With such a porous medium, the melting rate could be optimized by varying the height of a horizontal porous layer situated at the bottom of the cavity, where the melting rate is the lowest during convection-dominated melting. This height will be a function of the Rayleigh number. Since in the present experiments the right wall is held below the fusion temperature, the vertical porous layers apparently do not result in any significant advantage. However, for an adiabatic right wall, it is possible that the relatively low melting rates near the "end" of a canister could be increased by using a high porosity, high permeability vertical porous layer in this region.

CONCLUSIONS

An experimental study was conducted of melting in a rectangular enclosure filled with adjacent layers of a pure substance and a porous medium. The phase-change material was *n*-octadecane, and porous media composed of glass and aluminum beads of different size were investigated. Horizontal and vertical porous layers were considered. Rayleigh, Prandtl, and Stefan numbers were the same for all experiments. Variations in heat transfer and fluid flow between the experiments for each configuration were primarily due to differences in the permeability and effective thermal conductivity of the porous layers.

The experiments reveal two principal influences of the presence of the porous layer on solid-liquid phase change in the test cavity. The movement of the solid-liquid interface during the initial conduction-dominated melting period is faster in the porous medium than in the pure layer, owing to the lower porosity and higher effective thermal conductivity of the porous layer compared to those of the pure layer (with a porosity of unity). The porous layer also influences the melting process during the ensuing convection-dominated period. The lower permeability and higher effective thermal conductivity of the porous medium relative to the pure layer results in weaker convective flow in the porous layer than in the pure layer. In addition, the higher effective thermal conductivity results in a higher heat transfer rate across the remaining solid within the porous layer compared to the pure solid. Both of these phenomena cause faster movement of the solid-liquid interface in the pure layer than in the porous layer and sharp changes in the slope of the solid-liquid interface at the porous-pure layer interface. Overall, the shape of the solid-liquid interface in the pure region is relatively unaffected by the presence of the porous layer.

Differences in the thermophysical properties of the materials used for the porous layers affect the relative degree of influence of the porous layer on the melting processes in the cavity. A porous matrix of small beads and thus lower permeability result in weaker convective flow in the porous medium than a porous matrix of large beads. Therefore, in the convection-dominated melting period, the solid-liquid interface movement is slower in a porous layer of small beads. In a porous medium composed of beads of high thermal conductivity (ie, aluminum), the movement of the solid-liquid interface is faster than in a porous medium composed of beads of a lower thermal conductivity during times when the heat transfer in the pure and porous layers is conduction-dominated. Futhermore, the higher the effective thermal conductivity in the porous layer, the weaker the convective flow is in that layer, the lower the thermal resistance is across the remaining solid, and the sooner the melting process comes to steady state.

The melt volume fraction data reveal that none of the porous layers investigated results in an enhancement of the melting rate and thus in the heat transfer across the melt region compared to the experiment without a porous layer. This can be attributed to the relatively low porosity of the porous media tested as well as to the strong natural convection reduction caused by the low permeability of the porous layers. Both of the above effects are generally not offset by the relatively high effective thermal conductivities of the porous layers. Consequently, filling the entire test cell with the porous medium would have resulted in even lower melting rates. Therefore, it is of advantage to place a high thermal conductivity porous medium only in those regions of a thermal energy storage canister in which the melting rates are the lowest. It is recommended that porous media of higher porosity and permeability as well as larger ranges of the Rayleigh number be investigated.

The work reported in this paper was supported in part by the National Science Foundation under grant No. CBT-8808888.

NOMENCLATURE

- c specific heat, J/(kg · K)
- Da Darcy number ($= K/L^2$), dimensionless
- Fo Fourier number ($= \alpha_l t/L^2$), dimensionless
- g gravitational acceleration, m/s^2
- Δh latent heat of fusion, J/(kg · K)
- k thermal conductivity, $W/(m \cdot K)$
- K permeability, m^2
- L length of enclosure, m
- Pr Prandtl number ($= \nu_l/\alpha_l$), dimensionless
- Ra Rayleigh number [$= g\beta(T_H - T_C)L^3/\nu_l\alpha_l$], dimensionless
- Ste Stefan number [$= c_l(T_H - T_C)/\Delta h$], dimensionless
- t time, s
- T temperature, K
- V^* melt volume fraction (= vol melted PCM/test cell volume), dimensionless
- x horizontal coordinate, m
- y vertical coordinate, m

Greek Symbols

- α thermal diffusivity, m^2/s
- β coefficient of thermal expansion, K^{-1}
- γ volume fraction liquid in the phase change material, dimensionless
- ϵ porosity of the porous medium, dimensionless
- η vertical coordinate ($= y/L$), dimensionless
- θ temperature [$= (T - T_C)/(T_H - T_C)$], dimensionless

Λ thermal conductivity ratio ($= k_{\text{eff}}/k_l$), dimensionless
ν kinematic viscosity, m^2/s
ξ horitzonal coordinate ($= x/L$), dimensionless
ζ density, kg/m^3
Ω thermal capacitance ratio ($= \overline{\rho c}/\rho_l c_l$), dimensionless

Subscripts

b bead
C cold
eff effective
f fusion
H hot
i initial
l liquid
p porous
pcm phase-change material
s solid

REFERENCES

1. Henze, R. H., and Humphrey, J. A. C., Enhanced Heat Conduction in Phase-Change Thermal Energy Storage Devices, *Int. J. Heat Mass Transfer,* **24,** 459-474, 1981.
2. Spanner, G. E., and Wilfert, G. L., Potential Industrial Applications for Composite Phase-Change Materials as Thermal Energy Storage Media, DOE Report DE-89-015170, Pacific Northwest Laboratory, Richland, Wash., 1989.
3. Crane, R. A., Thermal Evaluation of Advanced Solar Dynamic Heat Receiver Performance, NASA Report CR-185117, Lewis Research Center, Cleveland, Ohio, 1989.
4. Strumpf, H. J., and Coombs, M. G., Advanced Heat Receiver Conceptual Design Study, NASA Report CR-180901, Lewis Research Center, Cleveland, Ohio. 1987.
5. Viskanta, R., Natural Convection in Melting and Solidification, in *Natural Convection: Fundamentals and Applications,* S. Kakac, W. Aung, R. Viskanta, Eds., pp. 845-877, Hemisphere, Washington, D.C., 1985.
6. Fukusako, S., and Seki, N., Fundamental Aspects of Analytical and Numerical Methods on Freezing and Melting Heat-Transfer Problems, *Ann. Rev. Num. Fluid Mech. Heat Transfer,* **1,** 351-402, 1987.
7. Yao, L. S., and Prusa, J., Melting and Freezing, in *Adv. Heat Transfer,* **19,** 1-95, 1989.
8. Marshall, R. H., Natural Convection Effects in Rectangular Enclosures Containing a Phase Change Material, in *Thermal Storage and Heat Transfer in Solar Energy Systems,* F. Kreith, R. Boehm, J. Mitchell, R. Bannerot, Eds., pp. 61-69, Am. Soc. Mechanical Engineers, New York, 1978.
9. Ho, C. J., and Viskanta, R., Experimental Study of Melting in a Rectangular Cavity, in *Proceedings of the Seventh International Heat Transfer Conference,* U. Grigull, E. Hahne, K. Stephan, J. Staub, Eds., Vol. 2, pp. 369-374, Hemisphere, Washington, D. C., 1982.
10. Bénard, C., Gobin, D., and Zanoli, A., Moving Boundary Problem: Heat Conduction in the Solid Phase of a Phase-Change Material During Melting Driven by Natural Convection in the Liquid, *Int. J. Heat Mass Transfer,* **29,** 1669-1681, 1986.
11. Goldstein, M. E., and Reid, R. L., Effect of Fluid Flow on Freezing and Thawing of Saturated Porous Media, *Proc. Roy. Soc. Lond. A,* **364,** 45-73, 1978.
12. Frivik, P. E., and Comini, G., Seepage and Heat Flow in Soil Freezing, *ASME J. Heat Transfer,* **104,** 323-328, 1982.
13. Weaver, J. A., and Viskanta, R., Freezing of Water Saturated Porous Media in a Rectangular Cavity, *Int. Commun. Heat Mass Transfer,* **13,** 245-252, 1986.
14. Beckermann, C., and Viskanta, R., Natural Convection Solid/Liquid Phase Change in Porous Media, *Int. J. Heat Mass Transfer,* **31,** 35-46, 1988.
15. Arquis, E., and Caltagirone, J. P., Interacting Convection Between Fluid and Open Porous Layers, ASME Paper 87-WA/HT-24, Am. Soc. Mechanical Engineers, New York, 1987.
16. Arquis, E., Caltagirone, J. P., and Langlais, C., Natural Convection in Cavities Partially filled with Permeable Porous Materials, in *Proceedings of the Eighth International Heat Transfer Conference,* C. L. Tien, V. P. Carey, J. K. Ferrell, Eds., pp. 2653-2658, Hemisphere, Washington, D.C., 1986.
17. Beckermann, C., Viskanta, R., and Ramadhyani, S., Natural Convection in Vertical Enclosures Containing Simultaneously Fluid and Porous Layers, *J. Fluid Mech.,* **186,** 257-284, 1988.
18. Ellinger, E. A., Solid/Liquid Phase Change Driven by Natural Convection in an Enclosure Partially Occupied by a Porous Medium, M.S. Thesis, Univ. Iowa, Iowa City, Iowa, 1989.
19. Veinberg, A. K., Permeability, Electrical Conductivity, Dielectric Constant, and Thermal Conductivity of a Medium with Spherical and Ellipsoidal Inclusions, *Sov. Phys. – Dokl.* **11,** 593-595, 1967.
20. Beckermann, C., and Viskanta, R., Effect of Solid Subcooling on Natural Convection Melting of a Pure Metal, *ASME J. Heat Transfer,* **111,** 416-424, 1989.

Received April 25, 1990; revised January 17, 1991